Chapter 11

Love Wave Biosensors: A Review

María Isabel Rocha Gaso, Yolanda Jiménez, Laurent A. Francis and Antonio Arnau

Additional information is available at the end of the chapter

http://dx.doi.org/10.5772/53077

1. Introduction

In the fields of analytical and physical chemistry, medical diagnostics and biotechnology there is an increasing demand of highly selective and sensitive analytical techniques which, optimally, allow an in real-time label-free monitoring with easy to use, reliable, miniaturized and low cost devices. Biosensors meet many of the above features which have led them to gain a place in the analytical bench top as alternative or complementary methods for routine classical analysis. Different sensing technologies are being used for biosensors. Categorized by the transducer mechanism, optical and acoustic wave sensing technologies have emerged as very promising biosensors technologies. Optical sensing represents the most often technology currently used in biosensors applications. Among others, Surface Plasmon Resonance (SPR) is probably one of the better known label-free optical techniques, being the main shortcoming of this method its high cost. Acoustic wave devices represent a cost-effective alternative to these advanced optical approaches [1], since they combine their direct detection, simplicity in handling, real-time monitoring, good sensitivity and selectivity capabilities with a more reduced cost. The main challenges of the acoustic techniques remain on the improvement of the sensitivity with the objective to reduce the limit of detection (LOD), multi-analysis and multi-analyte detection (High-Throughput Screening systems-HTS), and integration capabilities.

Acoustic sensing has taken advantage of the progress made in the last decades in piezoelectric resonators for *radio-frequency* (rf) telecommunication technologies. The so-called gravimetric technique [2], which is based on the change in the resonance frequency experimented by the resonator due to a mass attached on the sensor surface, has opened a great deal of applications in bio-chemical sensing in both gas and liquid media.

Traditionally, the most commonly used acoustic wave biosensors were based on QCM devices. This was primarily due to the fact that the QCM has been studied in detail for over 50 years and has become a mature, commercially available, robust and affordable technology [3, 4]. LW acoustic sensors have attracted a great deal of attention in the scientific community during the last two decades, due to its reported high sensitivity in liquid media compared to traditional QCM-based sensors. Nevertheless, there are still some issues to be further understood, clarified and/or improved about this technology; mostly for biosensor applications.

LW devices are able to operate at higher frequencies than traditional QCMs [5]; typical operation frequencies are between 80-300 MHz. Higher frequencies lead, in principle, to higher sensitivity because the acoustic wave penetration depth into the adjacent media is reduced [6]. However, the increase in the operation frequency also results in an increased noise level, thus restricting the LOD. The LOD determines the minimum surface mass that can be detected. In this sense, the optimization of the read out and characterization system for these high frequency devices is a key aspect for improving the LOD [7].

Another important aspect of LW technology is the optimization of the fluidics, specially the flow cell. This is of extreme importance for reducing the noise and increasing the biosensor system stability; aspects that will contribute to improve the LOD.

The analysis and interpretation of the results obtained with LW biosensors must be deeper understood, since the acoustic signal presents a mixed contribution of changes in the mass and the viscoelasticity of the adsorbed layers due to interactions of the biomolecules. A better understanding of the transduction mechanism in LW sensors is a first step to advance in this issue; however its inherent complexity leads, in many cases, to frustration [8].

The fabrication process of the transducer, unlike in traditional QCM sensors, is another aspect under investigation in LW technology, where features such as: substrate materials, sizes, structures and packaging must be still optimized.

This chapter aims to provide an updated insight in the mentioned topics focused on biosensors applications.

2. Basis of LW sensors

The Love wave physical effect was originally discovered by the mathematician Augustus Edward Hough Love. He observed an effect caused by earthquake waves far from the epicenter due to the lower acoustic wave velocity of waves propagating along the stratified geological layers [9]. The LW sensor is a layered structure formed, basically, by a piezoelectric substrate and a guiding layer (see Figure 1a). LW devices belong to the family of *surface acoustic wave* (SAW) devices in which the acoustic wave propagates along a single surface of the substrate. The piezoelectric substrate of a LW device primarily excites a *shear horizontal surface acoustic wave* (SH-SAW) or a *surface skimming bulk wave* (SSBW) depending on the material and excitation mode of the substrate. Both waves have shear horizontal particle dis-

placements (perpendicular to the wave propagation direction and parallel to the waveguide surface). This type of acoustic wave operates efficiently in liquid media, since the radiation of compressional waves into the liquid is minimized.

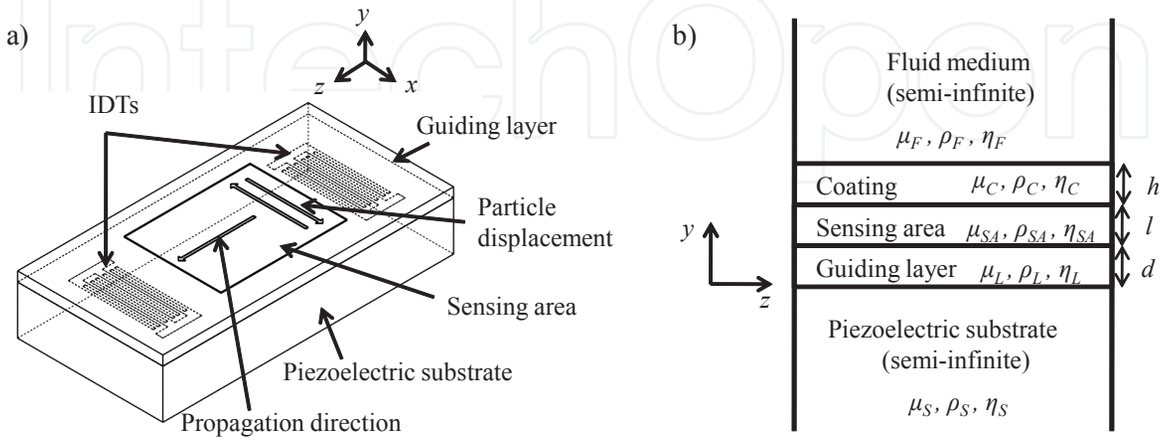

Figure 1. a) Basic structure of a LW sensor. b) Five-layer model of a LW biosensor.

LW sensors consist of a transducing area and a sensing area. The transducing area consists of the *interdigital transducers* (IDTs), which are metal electrodes, sandwiched between the piezoelectric substrate and the guiding layer. The input IDT is excited electrically (applying an rf signal) and launches a mechanical acoustic wave into the piezoelectric material which is guided through the guiding layer up to the output IDT, where it gets transformed back to a measurable electrical signal. The *sensing area* is the area of the sensor surface, located between the input and output IDT, which is exposed to the analyte.

LW sensors can be used for the characterization of processes involving several layers deposited over the sensing area; such is the case of biosensors. A LW biosensor can be described as a layered compound formed by the LW sensor in contact with a finite viscoelastic layer, the so-called coating, contacting a semi-infinite viscoelastic liquid as indicated in Figure 1b. Each layer has its material properties given by: the shear modulus μ, density ρ and viscosity η. Hence, the subscripts S, L, SA, C and F denotes the substrate, guiding layer, sensing area, coating and fluid layers, respectively. Biochemical interactions at the sensing area cause changes in the properties of the propagating acoustic wave which can be detected at the output IDT.

The difference between the mechanical properties of the guiding layer and the substrate creates an entrapment of the acoustic energy in the guiding layer keeping the wave energy near the surface and slowing down the wave propagation velocity. This guiding layer phenomenon makes LW devices very sensitive towards any changes occurring on the sensor surface,

such as those related to mass loading, viscosity and conductivity [5]. The higher the confinement of the wave in the guiding layer, the higher the sensitivity [10].

The proper design of a LW device for biosensor applications must consider the advances made on these basic elements. Updated information about each one of these elements is then required and can be found in the following sections.

2.1. Piezoelectric substrate

Thanks to *piezoelectricity* electrical charges can be generated by the imposition of mechanical stress. The phenomenon is reciprocal; applying an appropriate electrical field to a piezoelectric material generates a mechanical stress [11]. In LW sensors an oscillating electric field (rf signal) is applied in the input IDT which, due to the piezoelectric properties of the substrate, launches an acoustic guided wave. The guided wave propagates through the guiding layer up to the output IDT where, again due to the piezoelectric properties of the substrate, is converted back to an electric field for measurement. A remarkable parameter of the piezoelectric substrate is the *electromechanical coupling coefficient* (K^2), which indicates the conversion efficiency from electric energy to mechanical energy; its value depends on the material properties. This is an important design parameter in LW sensors, since higher K^2 lead to low loss LW devices and, therefore, more sensitive LW sensors [12].

When choosing a material for the substrate of LW devices, apart from the desired low losses, other requirements, such as low *temperature coefficient of frequency* (TCF) have to be considered as well. Special crystal cuts of the piezoelectric substrate material[1] can yield an intrinsically temperature-compensated device which minimizes the influence of temperature on the sensor response, thus improving the LOD [13,14].

The shear horizontal polarization required for operation of the LW sensor in liquid media is another aspect to be considered when choosing the substrate material. In this sense, quartz is the only common substrate material that can be used to obtain a *purely* shear polarized wave [13]. The crystal cut and the wave propagation direction, which depends on the IDTs orientation, define the elastic, dielectric and piezoelectric constants of the crystal, and therefore the wave polarization. Possible cuts which generate a purely shear polarized wave are the AT-cut quartz and the ST-cut quartz. AT-cut quartz and ST-cut quartz are both Y-cuts, rotated 35°15' and 42°45° about the original crystallographic X-axis, respectively.

Initially, LW devices were made in ST-cut quartz [15], however, ST-cut quartz is very sensitive to temperature (its TCF is around 40 ppm/°C) [16]. This was a restrictive factor in terms of sensor LOD and, thus, temperature-compensated systems based on different quartz cuts and different materials for the substrate such as lithium tantalate (LT), $LiTaO_3$, and lithium niobate (LN), $LiNbO_3$, were investigated [17-19]. In particular, AT-cut quartz, 36° YX LT and 36° YX LN were proposed, the last two corresponds to specific cuts of LT and LN materials [10]. Table 1 contains the values of some characteristic parameters of the previously men-

1 The substrate crystal cuts (or plates) are obtained by cutting slices of a single-crystal starting material with an arbitrary orientation relative to the three orthogonal crystallographic axes.

tioned substrate materials. In column 2, the *substrate shear velocity* v_S, is defined by the substrate material properties ($v_S = (\mu_S/\rho_S)^{1/2}$).

Substrate	v_S(m/s)	ρ_S(kg/m3)	K^2 (%)	TCF (ppm/°C)
ST-cut Z' propagating quartz	5050	2650	1.9	40
AT-cut Z' propagating quartz	5099	2650	1.4	0-1
36° YX LN	4800	4628	16	-75 to -80*
36° YX LT	4200	7454	5	-30 to -45

Table 1. Most commonly employed crystal cuts for LW devices (modified from [18]).*Approximate value.

LN substrates have higher coupling factor and low propagation loss than LT and quartz substrates. However, these substrates are extremely vulnerable to abrupt thermal shocks.

The low insertion loss, very large electromechanical coupling factor K^2 and low propagation loss which characterize 36° YX LT substrates [20] provide advantages over other substrates such as quartz cuts, where exquisite care in the fluidic packaging is required to prevent excessive wave damping [21]. For this reason, LT seems to be the substrate material of choice in high-loss applications due to its high coupling factor K^2, while in low-loss applications quartz may exhibit better wave characteristic [22]. The main shortcomings of 36° YX LT substrates are: they do not generate a pure shear wave, which increases the damping when is liquid loaded; and they have a poor thermal stability due to their high TFC (-30 to -40 ppm/°C [19]) if compared with AT-quartz.

From the point of view of thermal stability, AT-cut quartz seems to be the most appropriate due to its very low TCF [14]. Although the coupling coefficient of the AT-cut quartz is the lowest compared to other cuts, in our opinion, AT-cut quartz is currently the most suitable substrate for LW biosensing applications among the mentioned substrates, for several reasons: 1) it is capable of generating pure shear waves, diminishing the damping when is liquid loaded; 2) its thermal stability is the highest one, which improves the LOD; 3) the mass sensitivity of quartz substrates is significantly high than that of LT substrates [17,23]; and 4) LT and LN substrates are extremely fragile and must be handled with great care during the device fabrication to prevent them from breaking in pieces.

2.2. Interdigital transducers

Interdigital transducers (IDTs) were firstly reported in 1965 by White and Voltmer [24] for generating SAWs in a piezoelectric substrate. An IDT, in its most simple version, is formed by two identical combs-like metal electrodes whose strips are located in a periodic alternating pattern located on top of the piezoelectric substrate surface. Figure 2a shows the structure of a *single-electrode* IDT which consists of two strips per *period p* and *acoustic aperture W*. The strip width is equal to the space between strips (p/4). One comb is connected to ground

and the other to the center conductor of a coaxial cable where a rf signal is provided. A pair of two strips with different potential is called a *finger pair*.

The IDT electric equivalent circuit is explained in reference [25]. Figure 2b shows the IDT frequency response, where *A(f)* is the electrical amplitude of the rf signal. The maximum in *A(f)* occurs when the *wavelength* λ of the generated acoustic wave is equal to the period p and this arises at the so called *synchronous frequency* f_s. In relation to the *bandwidth B* of an IDT frequency response, this will be narrower when increasing the *number of finger pairs N*. However, there is a limitation in the maximum N recommended, due to the fact that, in practice, when N exceeds 100, the losses associated with mass loading and the scattering from the electrodes increase. This neutralizes any additional advantage associated with the increase of the number of the finger pairs.

Due to symmetry of the IDT in the direction of propagation, the LW energy is emitted in equal amounts in opposite directions, giving an inherent loss of 3 dB. In a two-port device this factor contributes 6 dB to the total insertion loss [25,26].

Aluminum has been widely used as IDTs material and has been extensibility demonstrated in literature as suitable for SAW generation. Aluminum has an ability to resist corrosion and is the third most abundant element on Earth (after oxygen and silicon). It also has a low cost compared to other metals. The metallic layer of the electrodes must be thick enough to present a low electric resistance, but sufficiently thin to avoid an excessive mechanic charge for the acoustic wave (acoustic impedance breaking) [27]. Generally, a thickness between 100 and 200 nm of aluminum is employed.

There are a number of second-order effects, which are often significant in practice, that affect the transducer frequency response. The effect for which the transducer strips reflect surface waves causing mechanical and electrical perturbations of the surface is called *electrode interaction* [30]. Usually, these unwanted reflections cancel each other over wide frequency bands and become negligible. However, in a certain frequency band, the scattered waves are in phase, adding them constructively and causing very strong reflection (*Bragg reflection*) which distorts the transducer frequency response. For a *single-electrode* IDT (see Figure 2a), this situation occurs at the resonance condition $\lambda = p$. Thus, *double-electrode* (or *double finger pair* or *split-electrode*) IDTs are used to avoid this unwanted effect. In double-electrode IDTs there are four strips per period (see Figure 2c) and thus, the Bragg reflection can be suppressed at the LW resonance frequency [28]. One disadvantage of the double-electrode is the increased lithographic resolution required for fabricating the IDTs [29].

Another significant second-order effect is the generation of the *triple-transit signal*. In a device using two IDTs, which is the case of a LW device, the output IDT will in general produce a reflected wave, which is then reflected a second time by the input IDT. Thus, a reflected wave reaches the output IDT after traversing the substrate three times, giving an unwanted output signal known as the *triple-transit signal* [26]. This effect is reduced by making the input and output IDT separation large enough.

Some authors use *reflectors* to improve the frequency response of the LW device. Reflectors are composed of metal gratings placed in the same configuration than IDTs and are located

at the ends of the IDTs (see Figure 2d). These components have generally less finger pairs than the IDTs. The space periodicity of the reflectors is equal than in the IDTs [30]. Very narrow low-loss pass band can be realized in a two-port device, when the device is designed so that the reflectors resonate at the IDT resonance frequency, since the transfer admittance becomes very large [28].

2.3. Guiding layer

The difference between the mechanical properties of the piezoelectric substrate and the guiding layer generates a confinement of the acoustic energy in the guiding layer, slowing down the wave propagation velocity, but maintaining the propagation loss [32]. In particular, the condition for the existence of Love wave modes is that the shear velocity of the guiding layer material ($v_L = (\mu_L/\rho_L)^{1/2}$) is less than that of the substrate ($v_S = (\mu_S/\rho_S)^{1/2}$) [31]. When both materials, substrate and guiding layer, have similar density the ratio $\mu_S/\ \mu_L$ determine the dispersion of the Love mode; a large value of that ratio (higher μ_S and lower μ_L) leads to a stronger entrapment of the acoustic energy [32] and thus, greater sensitivity. Hence, the benefit of the guiding layer is that an enhanced sensitivity to mass deposition can be obtained [33], but also to viscoelastic interactions.

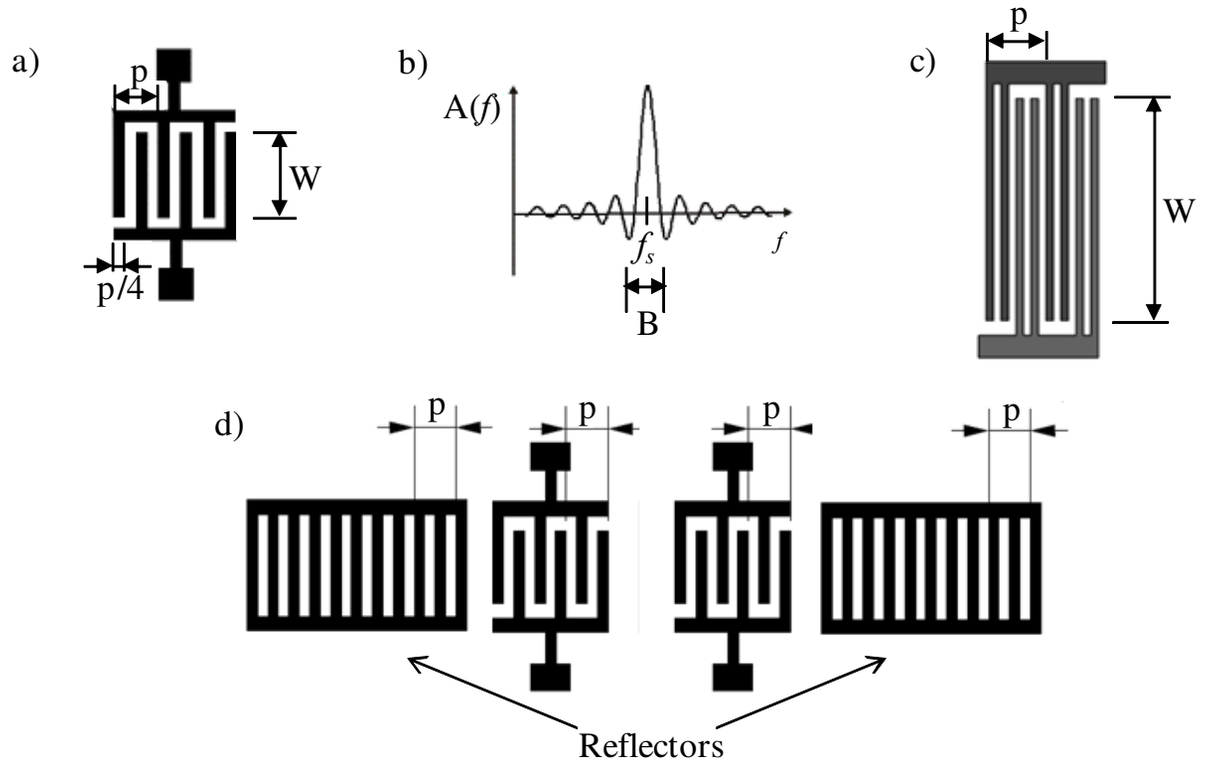

Figure 2. a) Single-electrode Interdigital Transducer (IDT) with period *p*, electrode width equal to space between electrodes (p/4) and aperture W (modified from [25]). b) Frequency response of an IDT (positive frequencies), where *A(f)* is the electrical amplitude (modified from [25]). c) Double-electrode IDT with period *p*, electrode width equal to space between electrodes and aperture W. d) Two grating reflectors are place at both ends of the IDTs (modified from [30]).

The effect of the guiding layer on Love modes influence the substrate coupling factor K^2, increasing it [14]. Also influence the temperature behavior, since modifies the TCF compared to their parent SSBWs device.

In relation to the materials used for the guiding layer, those with a low shear velocity and low insertion loss seem to be the most promising materials for developing sensitive biosensors [22,32,34]. Materials such as polymers [35], silicon dioxide (SiO_2) [17], gold (Au) [36] and zinc oxide (ZnO) [37,38] have been used as guiding layers [21]. In Table 2 some properties of these materials are presented[2]. The use of polymers (like Novolac, polyimide, polydimethylsiloxane (PDMS) and polymethylmethacrylate (PMMA)) is interesting from the point of view of the sensitivity, since they have low shear velocity. Additionally, some polymers, like Novolac photoresist, are very resistant to chemical agents [39,40]. However, polymers have high acoustic damping (losses) [39] and this is a clear disadvantage for biosensing application.

Guiding layer material	μ_L (GPa)	ρ_L (kg/m3)	v_L (m/s)
SiO_2	17.87	2200	2850.04
ZnO	40.17	5720	2650.00
Au	28.50	19300	1215.19
Polyimide	0.87	1420	780.48
PDMS	250×10^{-6}	965	16.09
PMMA	1.70	1180	1200.28

Table 2. Employed materials for guiding layers of LW devices.

Guiding layer/substrate structures made with ZnO as guiding layer have some advantages over those with a different material. This is the case of ZnO/ST-quartz structure, for which significantly high sensitivity, small TCF and high K^2 were reported [38]. ZnO/LT devices were also found to have higher mass sensitivity than SiO_2/LT [23]. However, ZnO has several disadvantages: it is CMOS contaminant, a semiconductor, and thus, it can deteriorate the efficiency of the transducers and make some artifacts. In addition, it gets easily rough when sputtered and it is very reactive with acids, liquids, or moisture, so it will dissolve if exposed to water or humid environment, which is a big problem in biosensors application. Regarding Au guiding layers, they provide very strong wave guiding, since Au has a relatively

2 These values are for guidance, since for deposited or grown materials these values depend on the desposition technique and for polymers layers on the cure process.

low shear acoustic velocity and a high density. However, it couples the rf signal from input to output IDT.

Silicon dioxide (SiO_2) -also known as fused silica- is a standard material in semiconductor industry and offers low damping, sufficient low shear velocity and excellent chemical and mechanical resistance [41]. It is the only native oxide of a common semiconductor which is stable in water and at elevated temperatures, an excellent electrical insulator, a mask to common diffusing species, and capable of forming a nearly perfect electrical interface with its substrate. When SiO_2 is needed on materials other than silicon, it is obtained by chemical vapor deposition (CVD), either thermal CVD or Plasma enhanced CVD (PECVD) [42]. The main shortcoming for SiO_2 is that the optimum thickness, at which the maximum sensitivity is reached, is very high (see Section 5), so this complicates the manufacturing process. Nevertheless, at the present, we consider that SiO_2 is the most appropriate material for LW biosensors guiding layer, mainly due to its low damping and excellent chemical and mechanical properties [42].

2.4. Sensing area

The sensing area can be made of different material than the guiding layer. Sensing layers have been reported composed of materials like PMMA [43] and SU-8 [44], but the most commonly employed is gold (Au). Generally, the thickness of this layer varies from 50-100 nm and 2-10 nm of chrome (Cr) or titanium (Ti) is needed to promote adherence to the guiding layer. Au surfaces are very attractive candidates for self-assembly due to their metallic nature, great nobility, and particular affinity for sulphur. This aspect allows functionalization with thiols of various types and adhesion to diverse organic molecules, which are modified to contain a sulphur atom. These coatings, assembled onto the gold surfaces, can serve as biosensors [36]. Immobilization techniques on gold for biosensing are quite common and much utilized in the scientific community. However, immobilization techniques on different materials, like SiO_2, could greatly simplify the LW biosensors fabrication.

3. Measurement techniques

Figure 3a shows a configuration of a two-port LW device where it behaves as a delay line. D is the distance between input and output IDT and L is the center-to-center distance between the IDTs. Thus, the sensor is a transmission line which transmits a mechanical signal (acoustic wave) launched by the input port (input IDT) due to the applied rf electrical signal. After a time delay the traveling mechanical wave is converted back to an electric signal in the output port (output IDT). In general, changes in the coating layer and/or in the semi-infinite fluid medium (see Figure 1b) produce variations in the acoustic wave properties (wave propagation velocity, amplitude or resonant frequency). These variations can be measured comparing the input and output electrical signal, since phasor V_{in} remains unchanged, while phasor V_{out} changes. Thus, from an electric point of view, a LW delay line can be defined by its transfer function $H(f) = V_{out}/V_{in}$, which repre-

sents the relationship between input and output electrical signal. *H(f)* is a complex number which can be defined as $H(f) = Ae^{j\varphi}$, being $A = |V_{out}/V_{in}|$ the amplitude and φ the *phase shift* between V_{out} and V_{in}. In terms of voltage, the *insertion loss* (*IL*) in dB is given by 20 $\log_{10}(A)$. Figure 3b, presents the frequency response of an AT-cut Z' propagating/SiO_2 LW device designed a fabricated by the authors of this chapter.

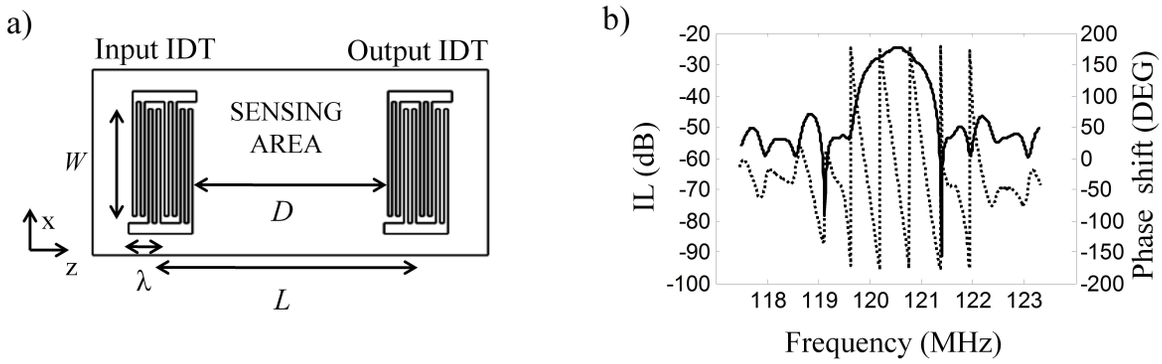

Figure 3. a) Scheme of a LW delay line. It consists of two ports. In the input IDT an rf signal is applied which launches an acoustic propagating wave. The output signal is recorded at the output IDT. *D* is the distance between input and output IDT and *L* is the center-to-center distance between the IDTs. b) Frequency response of a LW device designed a fabricated by the authors of this chapter. The phase shift (dotted line) and IL (solid line) were measured using a network analyzer.

In biosensors, biochemical interactions at the sensing area will modify the thickness and properties of the coating, and therefore variations in the amplitude and phase of the electrical transfer function can be measured. These variations can be monitored in real time, which provides valuable information about the interaction process.

The LW delay line can be used as frequency determining element of an oscillator circuit (*closed loop* configuration). Effectively, in an oscillator circuit the LW device is placed as a delay line in the feedback loop of an rf amplifier in a closed loop configuration [10,45]. Therefore, a change in the wave velocity, due to a sensing effect, produces a time delay in the signal through the LW device which appears as phase-shift; this phase-shift is transferred in terms of frequency-shift in an oscillator configuration. The oscillator is, apparently, the simplest electronic setup: the low cost of their circuitry as well as the integration capability and continuous monitoring are some features which make the oscillators an attractive configuration for the monitoring of the determining parameter of the resonator sensor, which in the case of the LW device is the phase-shift of the signal at resonance [46-49]. However, due to the following drawbacks, in our opinion, the oscillators are not the best option for acoustic wave sensor characterization: 1) they do not provide direct information about signal amplitude; 2) they, eventually, can stop oscillation if insertion losses exceed the amplifier gain during an experiment; and 3) despite of the apparent simple configuration, a very good design is necessary to guarantee that a LW resonator will operate at a specific frequency, and this is not a simple task. In effect, in the same way than in QCM oscillators it is required to assure that the sensor resonates on one defined resonance mode and does not "jump" be-

tween spurious resonances [7], in LW oscillators one must assure that the sensor will operate at one phase ramp in the sensor response band-pass, and does not jump from one to another which are almost of identical characteristics (see Figure 3b). Moreover, when the resonator dimensions get smaller and the frequency increases this becomes more difficult to achieve, since when increasing frequency there is a decrease of the resonator quality factor, a decrease in frequency stability [50] and in LW the ramps become nearer to each other.

In an *open loop* configuration, the input transducer is excited at a fixed frequency while the phase shift between V_{out} and V_{in}, φ, is recorded [32]. In this configuration, in the absence of interferences, phase variations measured experimentally can be related to changes in the physical properties of the layers deposited over the sensing area.

Network analyzers are the most commonly used instrumentation for characterizing LW delay lines in open loop configurations. Nevertheless, recently, some authors successfully validated a new characterization technique based on the open loop configuration [51]. A read out circuit based on this technique for high frequency liquid loaded QCM devices has been developed by the same authors [52], and tested with LW devices with very satisfactory results [53]. The main advantages of this read out circuit are its low cost, high integration, small size, calibration facility and the possibility of being used as an interface for multi-analysis detection.

4. Modeling methods

As mentioned, there is an open research field regarding the employed materials, and its physical and geometric properties for achieving more optimized LW devices for biosensors applications. For instance, the thickness of the Love-wave guiding layer is a crucial parameter that can be varied to achieve a more sensitivity device. The fabrication of LW sensors is complex and expensive due to their micro sizes [54]; therefore, simulations and modeling of LW devices as previous steps to their production could be very valuable. Models allow relating changes in some characteristics of the wave, as the velocity, with changes in the physical properties of the layers deposited over the sensing area, and thus, provide information about the sensing event. Nevertheless, modeling LW devices commonly requires simplified assumptions or the use of numerical methods [23] due to the complex nature of SAW propagation in anisotropic and piezoelectric materials.

In this section, information regarding the current most popular models used for modeling LW sensors is provided: the transmission line model, the dispersion equation and the Finite Element Method.

4.1. Transmission line model

It is well known that the propagation and attenuation of acoustic waves in guiding structures can be obtained by equivalent transmission line models [8,55]. The theory of sound wave propagation is very similar mathematically to that of electromagnetic waves, so tech-

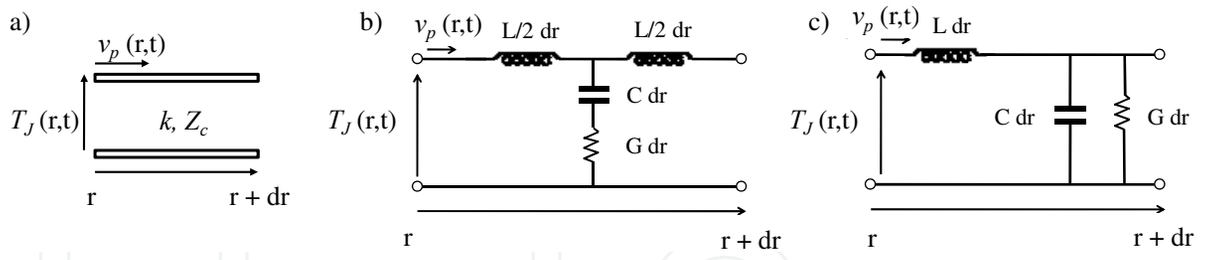

Figure 4. a) Pictorial representation of a transmission line. b) Transmission line equivalent series model for acoustic propagation in a viscoelastic layer. c) Transmission line equivalent parallel model for acoustic propagation in a viscoelastic layer.

niques from transmission line theory are also used to build structures to conduct acoustic waves; and these are also called transmission lines. The *transmission line model* (TLM) for acoustic waves take advantage of the concepts and techniques of proven value in electromagnetic microwaves to corresponding problems in elastic guided waves [8].

A transmission line is characterized by its *secondary parameters* which are the propagation *wavevector k* (when scalar *wavenumber*) and the *characteristic impedance* Z_c (see Figure 4a). It is important to mention that these parameters do not depend on the transmission line length. In each plane of an electric transmission line it is possible to define a magnitude for a voltage and other for the current in the line. For acoustics transmission lines current and voltage in electromagnetic are replaced by the *particle velocity* v_p and the *stress* $-T_J$, respectively, where J indicates de stress direction (J = 1, 2,..., 6) [55]. In an acoustic transmission line Z_c represents the relation between the stress $-T_J$ and the particle velocity v_p of the material, and k quantifies how the wave energy will be propagated along the transmission line. To quantify the variations of $-T_J$ and v_p when the wave propagates through the transmission line, the lumped elements models presented in Figure 4b and 4c are introduced. Figure 4b corresponds to the series model, and Figure 4c to the parallel model. The lumped elements of these models are called the transmission line *primary parameters*, which are dependent on the line length. Analyzing the parallel model of Figure 4c, the following coupled differential equations are obtained:

$$\frac{d^2T_J}{dr^2} = Z \cdot Y \cdot v_p$$
$$\frac{d^2v_p}{dr^2} = Z \cdot Y \cdot T_J \tag{1}$$

where $Z=j\omega L$, $Y=G+j\omega C$ and $\omega=2\pi f$. Being Z, L, Y, C, G, f, the impedance, inductance, admittance, capacitance and conductance per unit of length, respectively and f the frequency of T_J and v_p.

The solutions for these equations are given by:

$$T_J(\vec{r}) = T_J^{+} e^{-\gamma\cdot\vec{r}} + T_J^{-} e^{\gamma\cdot\vec{r}}$$
$$v_p(\vec{r}) = \frac{T_J^{+}}{Z_c} e^{-\gamma\cdot\vec{r}} - \frac{T_J^{-}}{Z_c} e^{\gamma\cdot\vec{r}} \quad (2)$$

where T^+ and T^- are arbitrary values for the intensity of the incident an reflected waves, respectively. The *linear propagation exponent* or *complex propagation factor* γ is directly related to the wavevector (γ=jk) and is given by $\gamma = (ZY)^{1/2} = \alpha + j\beta$. The real part of γ, denoted as *attenuation coefficient* α, represents the attenuation suffered by the wave when propagating through the transmission line. The imaginary part of γ, denoted as *phase coefficient* β, when multiplied by a distance, quantifies the phase shift that the wave suffers when traveling that distance. The characteristic impedance of the line Z_c is given by $Z_c=(Z/Y)^{1/2}$. First row of Table 3 shows the relationship between primary and secondary parameters of a transmission line for the series and parallel model.

The relation between the secondary (or primary) parameters and the properties of the transmission line materials is achieved by comparing Eqs. (1) with the motion equations of the LW assuming isotropic layers [55]. These relations are given in the second row of Table 3 for the series and parallel model.

Series model	Parallel model
$k = -j\gamma = \omega\sqrt{\frac{LC}{1 + j\omega C / G}}$ $Z_c = \sqrt{\frac{L}{C} + j\omega\frac{L}{G}}$	$k = -j\gamma = -j\sqrt{j\omega L\ (G + j\omega C)}$ $Z_c = \sqrt{\frac{j\omega L}{G + j\omega C}}$
$C = \frac{1}{\mu}$ $G = \frac{1}{\eta}$ $L = \rho$	$C = \frac{\mu}{\omega^2\eta^2 + \mu^2}$ $G = \frac{\eta\omega^2}{\omega^2\eta^2 + \mu^2}$ $L = \rho$

Table 3. Equivalent transmission line model parameters in terms of the layer properties.

Figure 5a shows a simplify description in which a LW propagates in a waveguide structure. Two assumptions were made: 1) the materials in the figure are isotropic (for piezoelectric substrates this assumption is valid because of a low anisotropy) and 2) the main wave propagating in the z direction results from the interaction of two partial waves with the same component in z direction and opposites components in y direction [12].

If all the properties of the layers which are involved in the LW transmission line are known, it is possible to obtain the *phase velocity of the Love mode* v_φ. The LW propagates in each layer i of the device in two directions z and y. In the case of a typical biosensor the device consists of 5 layers with the subscripts i equal to: S for the substrate, L for the guiding layer, SA for the sensing area, C for the coating and F for the fluid. Direction z is known as the *longitudinal direction* and direction y as the *transverse direction*. The wave does not find

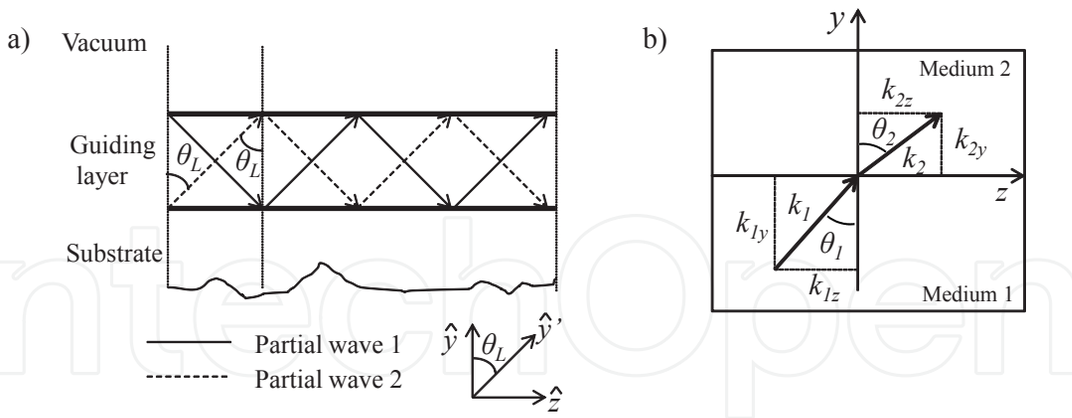

Figure 5. a) Simplified description of a LW traveling in a guided structure. b) Schematic representation of the wavevectors k_1 and k_2 in two different media.

any material properties change in the longitudinal direction; hence it propagates in this direction acquiring a phase shift and attenuation (in case of material with losses). However, in the transverse direction a stationary wave exists when the resonance condition is met. Thus, each layer counts with two transmission lines, one in the transverse direction and the other in the longitudinal direction. When a wave propagates in y' direction (see Figure 5a), as it happens with the partial waves of a layer i, k_i has that same direction (see Figure 5b), and therefore, it has components in z and y directions. In this way, the secondary parameters of each transmission line are determined from the projection of the parameter in the proper direction. The relation between the wavevector and the wave velocity is $k_i=\omega/v_i$. Therefore, k_i and v_i have the same directions, so the wave velocity in y' direction also has components in z and y.

Equations (3) and (4) give the expression of the secondary parameters and wave velocity in the transverse and longitudinal directions, respectively:

$$Z_{ciy} = Z_{ci}\cos\theta_i, \qquad k_{iy} = |k_i|\cos\theta_i, \qquad v_{iy} = |v_i|\cos\theta_i \tag{3}$$

$$Z_{ciz} = Z_{ci}\sin\theta_i, \qquad k_{iz} = |k_i|\sin\theta_i, \qquad v_{iz} = |v_i|\sin\theta_i \tag{4}$$

The angles θ_i are called *complex coupling angles* and depend on the material properties of each layer, but also on the material properties of the adjacent layers, since in each interface the Snell's laws have to be satisfied. In isotropic solids, the incident and reflected waves must all have the same component of k_i in the longitudinal direction [55]; therefore:

$$k_{Sz} = k_S\sin\theta_S = k_L\sin\theta_L = k_{Lz} = k_{SA}\sin\theta_{SA} = k_{SAz} = k_C\sin\theta_C = k_{Cz} = k_F\sin\theta_F = k_{Fz} \tag{5}$$

These conditions, together with the *transverse resonance relation* [8] obtained from the transmission line models in the direction of resonance (transverse direction) (see Figure 6) provides the phase velocity of the Love wave v_φ.

The transverse resonance relation establishes that:

$$\vec{Z}(P) + \vec{Z}(P) = 0 \tag{6}$$

where $\vec{Z}$ represents the acoustic impedance seen by the wave at the right of the plane P and $\vec{Z}$ the acoustic impedance seen by the wave at the left of the plane. This relation states that the acoustic impedances looking both ways from some reference plane P must sum to zero. The location of P is arbitrary. The solution of applying this condition provides an angle θ_i for one layer, depending on where P was located. From the material properties of each layer and applying the Snell's laws the angles for the rest of the layers can be found. Once these angles are known the z and y components of k_i and v_i can be obtained, and thus the phase velocity v_φ. Assuming that almost all the energy of the wave is confined in the waveguide, the phase velocity can be defined as the wavefront velocity of the acoustic wave propagating in the guiding layer, which in this case propagates in the z direction. In lossless materials k_{iz} and k_{iy} are real numbers and therefore v_φ is given by:

$$v_\varphi = \frac{\omega}{k_{Lz}} = \frac{\omega}{|k_L| \sin\theta_L} \tag{7}$$

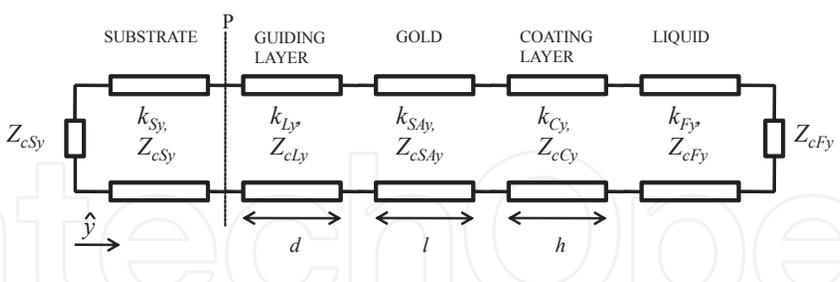

Figure 6. Equivalent transmission line model of the LW layered structure in the direction of resonance *y*. The lines are connected in series to satisfy the boundary conditions and the two semi-infinite layers are loaded with its characteristic impedance.

When the material has losses, k_{iz} and k_{iy} are complex numbers with real and imaginary parts, and then the attenuation coefficients appear:

$$k_i = k_{iz}\hat{z} + k_{iy}\hat{y} = \left(\beta_{iz} - j\alpha_{iz}\right)\hat{z} + \left(\beta_{iy} - j\alpha_{iy}\right)\hat{y} \tag{8}$$

In this case, the phase velocity is given by:

$$v_\varphi = \frac{\omega}{\beta_{Lz}} = \frac{\omega}{\Re\{k_{Lz}\}} = \frac{\omega}{\Re\{|k_L|\sin\theta_L\}} = \frac{1}{\Re\left\{\frac{\sin\theta_L}{|v_L|}\right\}} \tag{9}$$

On the other hand, the *attenuation of the Love Wave* α_{LW} is considered to happen mostly in the propagation direction *z*, since in the resonance direction, *y*, a stationary wave takes place. Therefore:

$$\alpha_{LW} = \alpha_{Lz} = -\Im\{k_{Lz}\} = -\Im\{|k_L|\sin\theta_L\} \tag{10}$$

Thus, following this procedure it is possible to obtain the phase velocity and attenuation of a LW propagating in a layer. Nevertheless, to complete this, it is necessary to know the material properties of all the layers which integrate the LW device. However, when the device is used as a sensor, and in particular in biosensor applications, the coating layer properties are unknown parameters. Thus, quantifying the variations suffered by the mechanical and geometric layer properties over the sensing layer when measuring the electrical parameters is what is really interesting.

Variations in amplitude and phase of the transfer function $H(f) = V_{out}/V_{in}$ (due to perturbations in the acoustic wave) can be monitored in real-time. These perturbations can occur due to variations of the mechanical and geometrical properties of the layers deposited over the sensing area. Such physical changes affect the propagation factor of the wave, and thus, the attenuation and phase velocity of the Love Wave. Next, the relations between LW electrical parameters defined in Section 3 (φ and *IL*) and the complex propagation factor are explained.

The relation between the output and input voltage in a delay line (DL) of length *z* can be modeled by its transfer function $H_{DL}(f)$ in the following way:

$$H_{DL}(f) = e^{-\gamma z} \tag{11}$$

where γ corresponds to the propagation factor of the wave in the line, which in this case corresponds to that of the guiding layer in the *z* direction γ_{Lz}. Assuming that the transfer function of the input and output IDTs is equal to unit [26], the relation between the electrical signal in the output and input IDTs $H(f)$ is the same than the one for the delay line:

$$H(f) = \frac{V_{out}}{V_{in}} = \frac{|V_{out}|}{|V_{in}|}e^{j(\varphi_{out}-\varphi_{in})} = \frac{|V_{out}|}{|V_{in}|}e^{j\varphi} = e^{-\gamma_{Lz}z} = e^{-(\alpha_{Lz}+j\beta_{Lz})z} \tag{12}$$

Thus, taking into account the relations defined in Section 3, the normalized phase shift and *IL* are given by:

$$\frac{IL}{z} = -\alpha_{Lz} 20 \log e$$
$$\frac{\varphi}{z} = -\beta_{Lz} \tag{13}$$

The increment in *IL*/*z* and φ/*z* from a non perturbed state γ_{Lz0} to a perturbed state γ_{Lz1} is the following:

$$\Delta\frac{IL}{z} = \left(\alpha_{Lz1} - \alpha_{Lz0}\right) \cdot 20 \log e$$
$$\Delta\frac{\varphi}{z} = \beta_{Lz1} - \beta_{Lz0} \tag{14}$$

The last set of equations provides a relation between the experimental data and the physical parameters of the layers. The extraction of the layers physical parameters is a major problem. Assuming that the physical properties of the substrate, guiding layer, gold and fluid medium are known and that these properties do not change during the sensing process, which can be the case in biosensing, still the parameters of the coating layer are not known. In comparison, the wave propagation direction in QCM coincides with the resonant direction. Therefore, for low frequency QCM applications it is possible to assume that the biochemical interaction is translated to simple mass changes, since it is reasonable to assume that the thickness of the coating layer is acoustically thin. This simplifies enormously the parameters extraction. However, in LW sensors, this assumption is not valid, and then the only two experimental data obtained in LW devices (Eq. (14)) are not enough to extract the unknown parameters of the coating. This, together with the complex equations which relate the measured data with the material properties, results in a complex issue that, to our knowledge, is not yet solved. Hence, there is an open research field of great interest related to this issue.

4.2. Dispersion equation

The *dispersion equation* provides the wave phase velocity as a function of the guiding layer thickness. The procedure for obtaining this equation for a two-layer system (guiding layer and substrate) is detailed in reference [56]. Broadly, this equation is reached after imposing the boundary conditions to determine the constants appearing in the particle displacement expressions of the waveguide and the substrate. These displacements are the solution of the equation of motion in an isotropic and non-piezoelectric material. Af-

ter extensive algebraic manipulation [56], the dispersion equation for a two-layer system is found, resulting [57]:

$$\tan\left(k_{Ly}d\right)=\frac{\mu_S}{\mu_L}\sqrt{\frac{1-\left(v_\varphi^2/v_S^2\right)}{\left(v_\varphi^2/v_L^2\right)-1}} \tag{15}$$

where k_{Ly} is the guiding layer transverse wavenumber in y direction, given by:

$$k_{Ly}=\sqrt{\frac{\omega^2}{v_L^2}-\frac{\omega^2}{v_\varphi^2}} \tag{16}$$

Taking into account the relation between the frequency and wave wavelength, $f = v_\varphi/\lambda$, the argument of the tangent in Eq.(15) can be written as:

$$k_{Ly}d=2\pi v_\varphi\frac{d}{\lambda}\sqrt{\frac{1}{v_L^2}-\frac{1}{v_\varphi^2}} \tag{17}$$

where the ratio d/λ is the normalized guiding layer thickness.

From the dispersion equation, the phase velocity can be solved numerically. On the other hand, the *group velocity*, v_g, as a function of the normalized guiding layer thickness can also be determined from the phase velocity by the formula [34]:

$$v_g=v_\varphi\left(1+\frac{d/\lambda}{v_\varphi}\frac{\mathrm{d}v_\varphi}{\mathrm{d}\left(d/\lambda\right)}\right) \tag{18}$$

The phase velocity and group velocity of an AT-cut quartz/SiO_2 Z' propagating layered structure were calculated using the dispersion equation (Eq. (15)) solved numerically through the bisection method. The data used to solve the equation for this LW structure were: v_S = 5099 m/s, ρ_S = 2650 kg/m^3, v_L = 2850 m/s, ρ_L = 2200 kg/m^3 and λ = 40 μm. The respective shear modulus were obtained through $\mu_i = v_i^2\ \rho_i$. Results are depicted in Figure 7. This figure provides information about the changes in the wave phase velocity due to changes in the guiding layer thickness. Assuming that the perturbing mass layer deposited over the sensing area is of the same material than the guiding layer, this equation will provide information over the sensing event. Nevertheless, this assumption is far

from the biosensors reality, where the consideration of a five–layer model is required (see Figure 1b).

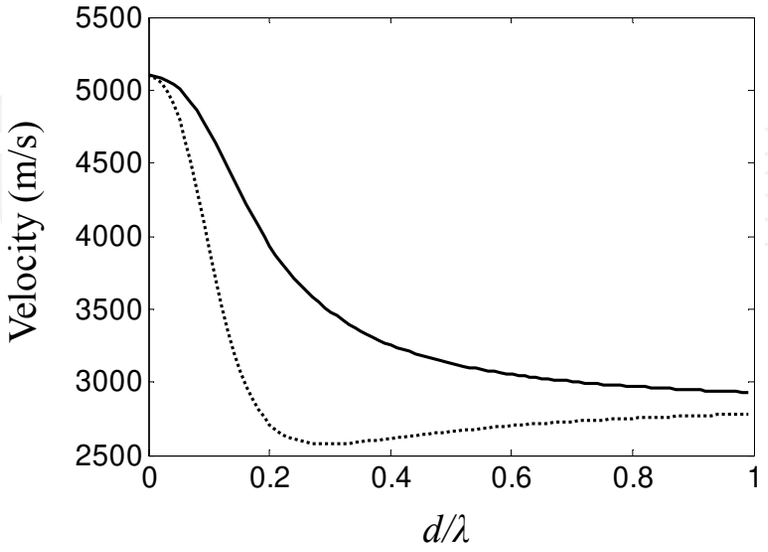

Figure 7. a) AT-cut Z' propagating quartz/SiO_2 phase velocity (continuous line) and group velocity (dashed line) for λ = 40 μm.

Mc Hale *et al*. developed the dispersion equation of three and four-layer systems neglecting piezoelectricity of the substrate [33]. When the substrate piezoelectricity is not considered, the dispersion equation is simplified. This can be the case of quartz substrates, which piezoelectricity is low. However, as the piezoelectricity of a substrate increases (like in the case of LT and LN), neglecting piezoelectricity, or assuming it is accounted for a stiffening effect in the phase velocity, may be less valid [58]. Liu et al. provided a theoretical model for analyzing the LW in a multilayered structure over a piezoelectric substrate [58]. Nevertheless, in our opinion, for those applications with a high number of layers, as in the case of biosensors, the use of the TLM is more convenient, since it is a very structured and intuitive model where the addition of an extra layer does not make the procedure more complex. From the programming point of view, this is an enormous advantage.

The phase velocity provided by the dispersion equation can be used to determine the optimal guiding layer thickness, which provides a maximum sensitivity. This issue will be addressed in Section 5.

4.3. LW sensor 3D FEM simulations

The models mentioned before, applied simplifying assumptions like considering the device substrate as isotropic and neglecting the substrate piezoelectricity. This makes the models far from the LW device reality. For a more accurate calculation of piezoelectric devices operating in the sonic and ultrasonic range, numerical methods such as finite element method (FEM) or boundary element methods (BEM) are the preferred choices [59]. The combination of the FEM and BEM (FEM/BEM) has been used by many authors for the simulation of SAW

devices [60]. Periodic Green's functions [61] are the basis of this model. However, the FEM/BEM only applies to infinite periodic IDTs and it is a 2 dimensional (2D) analysis. Thus, this method is only an approximation of a real finite SAW device.

Simulations of piezoelectric media require the complete set of fundamental equations relating mechanical and electrical phenomena in 3 dimensions (3D). The 3D-FEM can handle these types of differential equations. The FEM formulation for piezoelectric SAW devices is well explained in [59]. In general, the procedure for simulating LW devices using the 3D-FEM is the following: 1) the 3D model of the device is build using a computer-aided design (CAD) software; 2) the 3D model is imported to a commercial finite element software, which allows piezoelectric analysis; 3) the material properties of the involved materials are introduced in the software; 4) the convenient piezoelectric finite element is selected; 5) the model is meshed with the selected finite element; and 6) the simulation is run in the software. As result the software obtains the particle displacements and voltage at every node of the model.

Although 3D-FEM simulations are extremely useful tools for studying LW device electro-acoustic interactions, LW simulations in real size are still a challenge. Delay lines in practice are of many wavelengths and simulate them would require having too many finite elements. Thus, further efforts are required in order to achieve simulations able to reproduce real cases, which do not consume excessive computational resources. Nevertheless, some authors have simulated scaled LW sensors using this method [62-65].

5. Sensitivity and limit of detection

A key parameter when designing a LW biosensor is the device sensitivity [13]. In general terms, the sensitivity is defined as the derivative of the response (R) with respect to the physical quantity to be measured (M):

$$S = \lim_{\Delta M \to 0} \frac{\Delta R}{\Delta M} = \frac{dR}{dM} \tag{19}$$

It is possible to have different units of sensitivity depending on the used sensor response. E.g. for frequency output sensors, frequency ($R = f$), relative frequency ($R = f / f_0$), frequency shift ($R = f - f_0$) and relative frequency shift ($R = (f - f_0)/ f_0$) can be found, being f_0 the non perturbed starting frequency. Hence, four different possibilities of sensitivity formats are possible, and therefore it is extremely important to mention which case is been used in each application.

The sensitivity of LW sensors gives the correlation between measured electric signals delivered by the sensor and a perturbing event which takes place on the sensing area of the sensor. A high sensitivity relates a strong signal variation with a small perturbation [32]. Depending on the used electronic configuration, the electrical signal measured in LW devi-

ces can be: operation frequency, amplitude (or Insertion Loss), and phase. From this signal, and using the theoretical models, the phase velocity and group velocity can be obtained (see Sections 4.1 and 4.2).

When the sensor response R is the phase velocity, and the perturbing event which takes place on the sensing area is a variation of the *surface mass density* of the coating σ ($\sigma=h\ \rho_C$), the *velocity mass sensitivity* S^v_σ of a LW device at a constant frequency is given by [32,66]:

$$S_\sigma^v = \frac{1}{v_{\varphi 0}} \frac{\partial v_\varphi}{\partial \sigma}\bigg|_f \tag{20}$$

where $v_{\varphi 0}$ is the unperturbed phase velocity and v_φ is the phase velocity after a surface mass change.

Hence, S^v_σ has units of m^2/kg. In Eq. (20) partial derivatives have been considered as the phase velocity depends on several variables. The surface mass sensitivity reported for LW devices in literature are between 150-500 cm^2/g [45,67].

In sensor applications the phase velocity shift must be obtained from the experimental values of phase or frequency shifts. For the closed loop configuration, where the experimentally measured quantity is the frequency, the *frequency mass sensitivity* S^f_σ is defined as:

$$S_\sigma^f = \frac{1}{f_0} \frac{df}{d\sigma} \tag{21}$$

Jakoby and Vellekoop [66] noticed that the sensitivity measured by frequency changes in an oscillator (Eq. (21)) differs from the estimated velocity mass sensitivity (Eq. (20)) by a factor v_g/v_φ, since Love modes are dispersive. Thus, a typical 10% difference can be noted between S^f_σ and S^v_σ.

For the open loop configuration, where the experimentally measured quantity is the phase, the *phase sensitivity* (also called *gravimetric sensitivity*) S^φ_σ in absence of interference is defined as:

$$S_\sigma^\varphi = \frac{1}{k_{Lz} D} \frac{d\varphi}{d\sigma} = S_\sigma^v \tag{22}$$

where D is the distance between input and output IDT (see Figure 3) and k_{Lz} is the wavenumber of the Love mode, therefore $k_{Lz}D$ is the unperturbed phase φ_0.

The theoretical mass sensitivity of LW devices, derived from the perturbation theory[55], can be determined from the phase velocity according to [57]:

$$S_{\sigma}^{v} = \frac{-1}{\rho_L d}\left(1 + \frac{\sin(k_{Ly}d)\cos(k_{Ly}d)}{k_{Ly}d} + \frac{\rho_S}{\rho_L}\frac{\cos^2(k_{Ly}d)}{k_{Sy}d}\right)^{-1} \tag{23}$$

where k_{Ly} is the wavenumber in the guiding layer (Eq. (16)) and k_{Sy} is the wavenumber in the substrate (Eq. (24)). The minus sing in Eq. (23) indicates that the phase velocity of the perturbed event due to an increment in the surface mass density is less than the unperturbed phase velocity ($\Delta v_{\varphi} = v_{\varphi} - v_{\varphi 0}$).

$$k_{Sy} = \sqrt{\frac{\omega^2}{v_{\varphi}^{\,2}} - \frac{\omega^2}{v_S^{\,2}}} \tag{24}$$

The phase velocity can be obtained with the dispersion equation (see Figure 7) or transmission line model. Once the phase velocity is known, the mass sensitivity curve can be obtained using Eq. (23). In Figure 8, the dependence of the sensitivity with the guiding layer thickness for an AT-cut quartz/SiO_2 Z′ propagating structure is depicted. A maximum mass sensitivity S^{v}_{σ} of -39.44 m^2/kg is observed at d/λ of 0.171 which corresponds to a d = 6.84 μm. The phase velocity at d/λ = 0.171 is v_{φ} = 4140 m/s (see Figure 7) which leads to a synchronous frequency $f_s = v_{\varphi}/\lambda$ = 103.5 MHz.

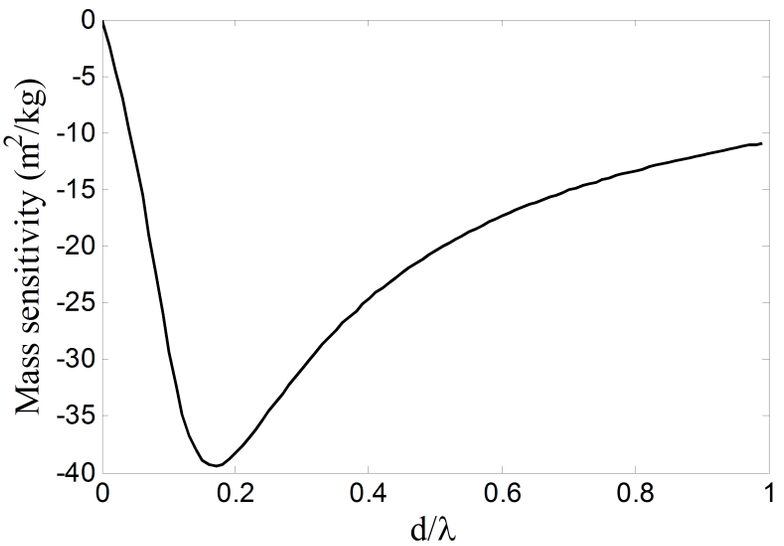

Figure 8. a) AT-cut quartz Z′ propagating /SiO_2 mass sensitivity considering λ = 40 μm.

Thus, as mentioned previously, for very small thicknesses compared to the wavelength, the acoustic field is not confined to the surface and deeply penetrates into the piezoelectric substrate, resulting in low mass sensitivity [68]. If the thickness is increased the sensitivity rises,

as the acoustic energy is more efficiently trapped in the guiding layer. However, an excessive increase in the guiding layer thickness leads to a reduction of wave energy density and the mass sensitivity decreases [69]. Therefore, there is an optimal guiding layer thickness at which a maximum mass sensitivity is achieved for a specific wavelength.

In those applications where a coating layer in contact with a liquid is deposited over the sensing area, such is the case for biosensors, both changes in the surface mass density $\Delta\sigma$ and in the mass viscosity $\Delta(\rho_C\eta_C)^{1/2}$ of the coating occur, due to the biochemical interaction between the coating and the liquid medium. In this case, the sensitivity can be modeled by the four components matrix shown in Eq.(25) [15]. These components relate shifts in surface mass density and in mass viscosity to the measured electrical signals: *phase shift* φ and *Insertion Loss (IL)*. The matrix components relate shifts of surface density $\Delta\sigma$ and mass viscosity $\Delta(\rho\eta)^{1/2}$ to shifts of electrical phase $\Delta\varphi$ and signal attenuation ΔIL. Notice that $S_{\varphi,\sigma}$ is not the same than S^{φ}_{σ} in Eq.(22).

$$\begin{bmatrix} \Delta\varphi \\ \Delta IL \end{bmatrix} = \begin{pmatrix} S_{\varphi,\sigma} & S_{\varphi,\sqrt{\rho_C\eta_C}} \\ S_{IL,\sigma} & S_{IL,\sqrt{\rho_C\eta_C}} \end{pmatrix} \begin{bmatrix} \Delta\sigma \\ \Delta\sqrt{\rho_C\eta_C} \end{bmatrix} \tag{25}$$

Generally, the high sensitivity of microacoustic sensors is closely related to the fact that they show a high temperature stability (low TCF) and a large signal-to-noise ratio, which, in turn yields low detection limits and a high resolution of the sensor [13]. The *limit of detection* (LOD) is a very important characteristic of acoustic biosensors, since it gives the minimum surface mass that can be detected by the device. It can be directly derived from the ratio between the noise in the measured electrical signal N_f and the sensitivity of the device. For instance, in a closed loop configuration, this noise N_f is the RMS value of the frequency measured over a given period of time in stable and constant conditions [32]. It is usually recommended to measure a signal variation higher than 3 times the noise level in order to conclude from an effective variation [70]. From this recommendation, it comes out that the LOD is given by [32,71]:

$$\mathrm{LOD} = \sigma_{\min} = \frac{3 \cdot N_f}{S_{\sigma}^{f} \cdot f} \tag{26}$$

where f is the operation frequency.

The LOD is improved by minimizing the influence of temperature on the sensor response [13]. The stability with respect to temperature can be achieved by implementing temperature control in the biosensor system and choosing materials of low TCF, as seen in Section 2.1.

6. LW packaging and flow cells

Flow cells are usually constructed with an inlet at one side, an outlet at the other, and the channels facing the sensor (see Figure 9). In most cases, a rubber seal is used for sealing, and in LW flow-cells additional absorbers made with rubber materials at the ends of the IDTs are recommended to improve the signal response (see Figure 9b). Factors such as the flow cell design, flow patterns and flow-through system influence the binding efficiency and the course of binding kinetics, resulting in possible variations of the true results [72].

The permittivity and the dielectric losses of the liquid medium, necessary in LW biosensors applications, influence the propagation of Love modes, since this medium acts as an additional layer. When the liquid medium is deposited over the device surface, the presence of this medium over the IDTs modifies the electrodes transfer function [73]. Permittivity and dielectric losses of the liquid lead to a corresponding change of the IDT input admittance, which influences the amplitude of the signal. A flow–through cell is crucial to eliminate this electric influence of the liquid. Such flow-cell isolates the IDTs from the liquid, confining the liquid in the region between the IDTs (sensing area). LW device packaging or flow-cells generally use walls to accomplish this purpose. These walls, when pressed onto the device surface, disturb the acoustic wave, resulting in an increase in overall loss and distortion of the sensor response. Walls must be designed to minimize the contact area in the acoustic path in order to obtain the minimum acoustic attenuation (see Figure 9c). It is known that the acoustic wave is significantly affected when increasing the walls width [27] and that materials used for these walls play an important role. Hence, great care must be taken to ensure that the designed LW flow cells do not greatly perturb the acoustic signal. Recently, some researchers have explored different possibilities to achieve the packaging of LW sensors for fluidic applications [27,74] and other authors have being exploring different LW flow-cell approaches [53,75,76].

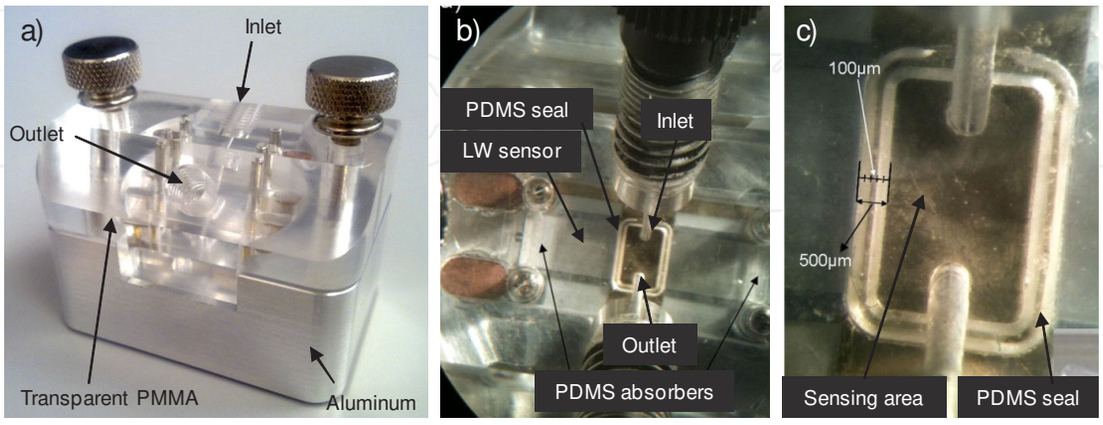

Figure 9. A developed LW flow cell for immunosensors application designed and fabricated by the authors of this chapter [53]. a) Overview of the flow cell b) Microscope view through the PMMA of the LW sensor and flow cell elements. c) PDMS square seal with pick end to minimize the contact area.

Further improvements for LW biosensors flow cells can be achieved, since it is an entirely new field and the development trends moves towards smaller flow cells which allows the use of less analyte. For instance, investigation on the materials used for creating flow cells, packaging, and flow patterns in microfluidic channels [72] would enhance LW performance and move them faster to the lab-on-a-chip arena.

7. LW biosensors state-of-the-art

The first approaches employing LW for biochemical sensing were reported in 1992 by Kovacs et al. [77] and by Gizeli et al. [78], who first demonstrated the use of such devices as mass sensing biosensors in liquids. However, it was not until 1997 that LW acoustic devices were used to detect real-time antigen-antibody interactions in liquid media [46].

In 1999, a contactless LW device was built in order to protect electrodes from the conductive and chemically aggressive liquids used in biosensing [79]. The advantage of this technique is that no bonding wires are required.

In 2000, a dual channel LW device was used as a biosensor to simultaneously detect *Legionella* and *E. coli* by Howe and Harding [80]. In this approach a novel protocol for coating bacteria on the sensor surface prior to addition of the antibody was introduced. Quantitative results were obtained for both species down to 10^6 cells/mL, within 3 h.

In 2003, a LW immunosensor was designed as a model for virus or bacteria detection in liquids (drinking or bathing water, food, etc.) by Tamarin et al. [47]. They grafted a monoclonal antibody (AM13 MAb) against M13 bacteriophage on the device surface (SiO_2) and sensed the M13 bacteriophage/AM13 immunoreaction. The authors suggested the potentialities of such acoustic biosensors for biological detection. The same year, it was shown that mass sensitivity of LW devices with ZnO layer was larger than that of sensors with SiO_2 guiding layers [48]. The authors of this work monitored adsorption of rat immunoglobulin G, obtaining mass sensitivities as high as 950 cm^2/g. They pointed out that such a device was a promising candidate for immunosensing applications.

An aptamer-based LW sensor which allowed the detection of small molecules was developed by Schlensog et al. in 2004 [81]. This biosensor offers an advantage over immunosensors, since it does not require the production of antibodies against toxic substances. A LW biosensor for the detection of pathogenic spores at or below inhalational infectious levels was reported by Branch et al. in 2004 [20]. A monoclonal antibody with a high degree of selectivity for anthrax spores was used to capture the non-pathogenic simulant *Bacillus thuringiensis* B8 spores in aqueous conditions. The authors stated that acoustic LW biosensors will have widespread application for whole-cell pathogen detection.

Moll et al. developed an innovative method for the detection of *E. coli* employing an LW device in 2007 [49]; it consisted of grafting goat anti-mouse antibodies (GAM) onto the sensor surface and introducing *E. coli* bacteria mixed with anti-*E. coli* MAb in a second step. The sensor response time was shorter when working at 37°C, providing results in less than 1

hour with a detection threshold of 10^6 bacteria/mL. More recently, the same group described a multipurpose LW immunosensor for the detection of bacteria, virus and proteins [82]. They successfully detected bacteriophages and proteins down to 4 ng/mm^2 and *E.coli* bacteria up to 5.0×10^5 cells in a 500 μL chamber, with good specificity and reproducibility. The authors stated that whole bacteria can be detected in less than one hour.

Andrä et al. used a LW sensor to investigate the mode of action and the lipid specificity of human antimicrobial peptides [83]. They analyzed the interaction of those peptides with model membranes. These membranes, when attached to the sensor surface, mimic the cytoplasmic and the outer bacterial membrane. A LW immunosensor was used in 2008 by Bisoffi et al. [84] to detect Coxsackie virus B4 and Sin Nombre Virus (SNV), a member of the hantavirus family. They described a robust biosensor that combines the sensitivity of SAW at a frequency of 325 MHz with the specificity provided by monoclonal and recombinant antibodies for the detection of viral agents. Rapid detection (within seconds) for increasing virus concentrations was reported. The biosensor was able to detect SNV at doses lower than the load of virus typically found in a human patient suffering from hantavirus cardiopulmonary syndrome.

In 2009, it was shown the possibility to graft streptavidin-gold molecules onto a LW sensor surface in a controlled way and was demonstrated the capability of the sensor to detect nano-particles in aqueous media by Fissi et al. [85]. In 2010, a complementary metal–oxide semiconductor CMOS-LW biosensor for breast cancer biomarker detection was presented by Tigli et al. [36]. This biosensor was fabricated using CMOS technology and used gold as guiding layer and as interface material between the biological sensing medium and the transducer.

LW devices were used as sensors for okadaic acid immono-detection through immobilized specific antibodies by Fournel et al. [76]. They obtained three times higher frequency shifts with the okadaic acid than with an irrelevant peptide control line. A LW based bacterial biosensor for the detection of heavy metal in liquid media was reported in 2011 by Gammoudi et al. [86]. Whole bacteria (*E. coli*) were fixed as bioreceptors onto the acoustic path of the sensor coated with a polyelectrolyte multilayer using a layer by layer electrostatic self-assembly procedure. Changes of bacteria viscoelastic equivalent parameters in presence of toxic heavy metals were monitorized.

A LW-based wireless biosensor for the simultaneous detection of Anti- Dinitrophenyl-KLH (anti-DNP) immunoglobulin G (IgG) was presented by Song et al. in 2011 [87]. They used poly(methyl-methacrylate) (PMMA) guiding layer and two sensitive films (Cr/Au). A LW sensor whose phase shifts as a function of the immobilized antibody quantity, combined with an active acoustic mixing device, was proposed by Kardous et al. [88] in 2011. They assessed that mixing at the droplet level increases antibodies transfer to a sensing area surface and increases the reaction kinetics by removing the dependency with the protein diffusion coefficient in a liquid, while inducing minimum disturbance to the sensing capability of the Love mode. LW sensors have been also used to study the properties of protein layers [40], DNA [89,90] and detect the adsorption and desorption of a lipid layer [91].

Currently, the only commercial LW biosensor system available in the market is commercialized by the German company *SAW instruments GmbH*. The sensor system can achieve a limit of detection (LOF) of 0.05 ng/cm^2 with a sample volume of 40-80 μL. *Senseor* company (Mougins, France) has a commercially available microbalance development kit (SAW-MDK1) which consists of a two-channel LW delay lines.

8. Trends and future challenges of LW sensors

LW biosensors have not been very well recognized by the scientific community [72] nor by the market yet. This might be due to the technological hindrances found for applying this device as biosensor, since it is sensitive to changes in the viscoelastic properties of the coating, which complicates the results interpretation. Reports about applications where mass alterations are separated from viscoelastic effects can enhance the acceptance of LW sensors [72]. Hence, it is necessary to investigate different alternatives for carrying out the procedure of parameters extraction with LW sensors. Nowadays, the trend is the placement of multiple, small, versatile sensors into a network configured for a specific location [10]. LW devices will move into the lab-on-a chip arena during the next years. Nevertheless, LW devices still have some hurdles to clear. LW biosensors packaging needs further development and cost reduction. In addition, much research and efforts are still required addressing the fluidic technology issue. Integration and automation with electronics and flow cells reduce costs of the system and increase the throughput. For a better performance of LW sensors, the combination with other detection methods such as optical [32] or chromatographic [92] are being considered.

Mathematical modeling and simulations of these devices are also essential for the development of new sensors, especially with respect to the study of new materials and wave propagation [72]. Numerical calculations and FEM analysis of LW sensors could help for further understanding of these devices.

Author details

María Isabel Rocha Gaso[1,2], Yolanda Jiménez[1], Laurent A. Francis[2] and Antonio Arnau[1]

*Address all correspondence to: marocga@doctor.upv.es

1 Wave Phenomena Group, Department of Electroic Engineering, Universitat Politècnica de València, Spain

2 Sensors, Microsystems and Actuators Laboratory of Louvain (SMALL), ICTEAM Institute, Université Catholique de Louvain, Belgium

References

[1] March C, Manclús JJ, Jiménez Y, Arnau A, Montoya A. A piezoelectric immunosensor for the determination of pesticide residues and metabolites in fruit juices. Talanta 2009;78(3) 827-833.

[2] Lucklum R, Soares D, Kanazawa K. Models for resonant sensors. In: Arnau A. (ed.) Piezoelectric transducers and applications. Springer; 2008. p63-96.

[3] Janshoff A, Galla HJ, Steinem C. Piezoelectric mass-sensing devices as biosensors- an alternative to optical biosensors? Angew. Chem. Int. Ed. 2000;39 4005-4032.

[4] Andle JC and Vetelino JF. Acoustic wave biosensors. Sens. Actuators, A 1994;44 167-176.

[5] Länge K, Rapp BE, Rapp M. Surface acoustic wave biosensors: a review. Anal. Bioanal. Chem. 2008;391(5) 1509-1519.

[6] Smith JP and Hinson-Smith V. Commercial SAW sensors move beyond military and security applications. Anal. Chem. 2006; 3505-3507.

[7] Weber J, Link M, Primig R, Pitzer D, Wersing W, Schreiter M. Investigation of the scaling rules determining the performance of film bulk acoustic resonators operating as mass sensors. IEEE Trans. Ultrason. Ferroelectr. Freq. Cont. 2007;54(2) 405-412.

[8] Oliner AA. Microwave network methods for guided elastic waves. IEEE Trans. Microwave Theory Tech. 1969;17(11) 812-826.

[9] Voinova MV. On Mass Loading and Dissipation Measured with Acoustic Wave Sensors: A Review. Journal of Sensors 2009; 1-13.

[10] Rocha-Gaso M-I, March-Iborra C, Montoya-Baides A, Arnau-Vives A. Surface generated acoustic wave biosensors for the detection of pathogens: a review. Sensors 2009;9 5740-5769.

[11] Ballato A. Piezoelectricity: old effect, new thrusts. IEEE Trans. Ultrason. Ferroelectr. Freq. Cont. 1995;42(5) 916-926.

[12] Francis LA. Investigation of Love waves sensors. Optimisation for biosensing applications. Master Thesis. Université Catholique de Louvain; 2001.

[13] Jakoby B, Bastemeijer J, Vellekoop MJ. Temperature-compensated Love-wave sensors on quartz substrates. Sens. Actuators, A 2000;82((1-3)) 83-88.

[14] Herrmann F and Büttgenbach S. Temperature-compensated Shear Horizontal surface acoustic wave in layered quartz/SiO_2- structures. Physica status solidi 1998;170 R3-R4.

[15] Du J and Harding GL. A multilayer structure for Love-mode acoustic sensors. Sens. Actuators, A 1998;65 152-159.

[16] Tamarin O, Déjous C, Rebiere D, Pistré J, Comeau S, Moynet D, Bezian J. Study of acoustic Love wave devices for real time bacteriophage detection. Sens. Actuators, B 2003;91 275-284.

[17] Herrmann F, Weihnacht M, Buttgenbach S. Properties of sensors based on shear-horizontal surface acoustic waves in LiTaO3/SiO2 and quartz/SiO2 structures. IEEE Trans. Ultrason. Ferroelectr. Freq. Cont. Jan.2001;48(1) 268-273.

[18] Kalantar-Zadeh K, Powell DA, Sadek AZ, Wlodarski W, Yang QB, Li YX. Comparison of ZnO/64° LiNbO3 and ZnO/36° LiTaO3 surface acoustic wave devices for sensing applications. Sens. Lett. 2006;4(2) 135-138.

[19] Hickernell FS, Knuth HD, Dablemont RC, Hickernell TS. The surface acoustic wave propagation characteristics of 64° YX $LiNbO_3$ and 36° YX $LiTaO_3$ substrates with thin-film SiO_2. In: proceedings of the IEEE Ultrason.Symp., Seattle, USA. 1995.

[20] Branch DW and Brozik SM. Low-level detection of a Bacillus anthracis simulant using Love-wave biosensors on 36° YX $LiTaO_3$. Biosens. Bioelectron. 2004;19 849-859.

[21] Branch DW and Thayne LE. 4D- 4 Love wave acoustic array biosensor platform for autonomous detection. In: proceedings of the IEEE Ultrason.Symp., 2007.

[22] Gizeli E, Bender F, Rasmusson A, Saha K, Josse F, Cernosek R. Sensitivity of the acoustic waveguide biosensor to protein binding as a funcion of the waveguide properties. Biosens. Bioelectron. 2003;18 1399-1406.

[23] Powell DA, Kalantar-Zadeh K, Wlodarski W. Numerical calculation of SAW sensitivity: application to ZnO/$LiTaO_3$ transducers. Sens. Actuators, A 2004;115 456-461.

[24] White RM and Voltmer FW. Direct piezoelectric coupling to surface elastic waves. Appl. Phys. Lett. 1965;7(12) 314-316.

[25] Nieuwenhuizen MS and Venema A. Surface acoustic wave chemical sensors. Sens. Mater. 1989;5 261-300.

[26] Morgan DP. Surface-Wave Devices for Signal Processing. Elsevier Science Publishers B.V.; 1991.

[27] El Fissi L. Détection et mesure de nanoparticules pour les applications de capteurs en milieu liquide. PhD Thesis. Université de Franche-Comté; 2009.

[28] Hashimoto K-Y. Surface Acoustic Wave Devices in Telecommunications. Springer-Verlag; 2000.

[29] Campbell C. Surface acoustic wave devices and their signal processing applications. Academic Press; 1989.

[30] Mazein P. Étude de dispositifs à ondes de Love par modélisation numérique de la propagation d'ondes acoustiques. Application à l'optimisation de structures et à la

caractérisation de matériaux en vue de la réalisation de capteurs chimiques. PhD Thesis. L'Université Bordeaux I; 2005.

[31] Du J, Harding GL, Ogilvy JA, Dencher PR, Lake M. A study of Love-wave acoustic sensors. Sens. Actuators, A 1996;56 211-219.

[32] Francis LA. PhD Thesis. Thin film acoustic waveguides and resonators for gravimetric sensing applications in liquid. PhD Thesis. Université Catholique de Louvain; 2006.

[33] McHale G, Newton MI, Martin F. Theoretical mass,liquid,and polymer sensitivity of acoustic wave sensorswith viscoelastic guiding layers. Appl. Phys. Lett. 2003;93(1) 675-690.

[34] Barié N, Wessa T, Bruns M, Rapp M. Love waves in SiO_2 layers on STW-resonators based on $LiTaO_3$. Talanta 2004;62 71-79.

[35] Gizeli E, Stevenson AC, Goddard NJ, Lowe CR. A novel Love-plate acoustic sensor utilizing polymer overlayers. IEEE Trans. Ultrason. Ferroelectr. Freq. Cont. 1992;39(5) 657-659.

[36] Tigli O, Binova L, Berg P, Zaghloul M. Fabrication and characterization of a Surface-Acoustic-Wave biosensor in CMOS Technology for cancer biomarker detection. IEEE Trans. Biomedical. Circuit. Systems. 2010;4(1) 62-73.

[37] Powell DA, Kalantar-Zadeh K, Ippolito S, Wlodarski W. 3E- 2 A layered SAW device based on $ZnO/LiTaO_3$ for liquid media sensing applications, 1 ed 2002, pp. 493-496.

[38] Kalantar-Zadeh K, Trinchi A, Wlodarski W, Holland A. A novel Love-mode device based on a ZnO/ST-cut quartz crystal structure for sensing applications. Sens. Actuators, A 2002;100 135-143.

[39] Matatagui D, Fontecha J, Fernández MJ, Aleixandre M, Gracia I, Cané C, Horrillo MC. Array of Love-wave sensors based on quartz/Novolac to detect CWA simulants. Talanta 2011;85 1442-1447.

[40] Saha K, Bender F, Rasmusson A, Gizeli E. Probing the viscoelasticity and mass of a surface-bound protein layer with an Acoustic Waveguide Device. Langmuir 2003;19 1304-1311.

[41] Herrmann F, Hahn D, Büttgenbach S. Separate determination of liquid density and viscosity with sagitally corrugated Love mode sensors. Sens. Actuators, A 1999;78 99-107.

[42] Franssila S. Introduction to Microbabrication. Wiley; 2004.

[43] Gizeli E, Liley M, Lowe CL. Design considerations for the acoustic waveguide biosensor. Smart Mater. Struct. 1997;6 700-706.

[44] El Fissi L, Friedt J-M, Ballandras S, Robert L, Chérioux F. Acoustic characterization of thin polymer layers for Love mode surface acoustic waveguide. In: proceedings of the IEEE Int.Freq.Control Symp., 2008.

[45] Grate JW, Stephen JM, Richard MW. Acoustic wave microsensors. Anal. Chem. 1993;65(21) 940A-848A.

[46] Harding GL, Du J, Dencher PR, Barnett D, Howe E. Love wave acoustic immunosensor operation in liquid. Sens. Actuators, A 1997;61(1-3) 279-286.

[47] Tamarin O, Comeau S, Déjous C, Moynet D, Rebière D, Bezian J, Pistré J. Real time device for biosensing: design of a bacteriophage model using love acoustic wave. Biosens. Bioelectron. 2003;18 755-763.

[48] Kalantar-Zadeh K, Wlodarski W, Chen YY, Fry BN, Galatsis K. Novel Love mode surface acoustic wave based immunosensors. Sens. Actuators, B 2003;91 143-147.

[49] Moll N, Pascal E, Dinh DH, Pillot JP, Bennetau B, Rebiere D, Moynet D, Mas Y, Mossalayi D, Pistre J, Dejous C. A Love wave immunosensor for whole E. coli bacteria detection using an innovative two-step immobilisation approach. Biosens. Bioelectron. Apr.2007;22(9-10) 2145-2150.

[50] Zimmermann B, Lucklum R, Hauptmann P, Rabe J, Büttgenbach S. Electrical characterisation of high-frequency thickness-shear-mode resonators by impedance analysis. Sens. Actuators, B 2001;76 47-57.

[51] Montagut Y, Garcia JV, Jimenez Y, March C, Montoya A, Arnau A. Validation of a phase-mass characterization concept and interface for acoustic biosensors. Sensors (Basel) 2011;11(5) 4702-4720.

[52] Montagut YJ, Garcia JV, Jimenez Y, March C, Montoya A, Arnau A. Frequency-shift vs phase-shift characterization of in-liquid quartz crystal microbalance applications. Rev. Sci. Instrum. 2011;82(6) 064702.

[53] Rocha-Gaso MI, March C, García J, El Fissi L, Francis LA, Jiménez Y, Montoya A, Arnau A. User-friendly love wave flow cell for biosensors. In: proceedings of the Biosensors 2012, Cancun, Mexico. 2012.

[54] Abdollahi A, Jiang A, Arabshahi SA. Evaluation on mass sensitivity of SAW sensors for different piezoelectric materials using finite-element analyisis. IEEE Trans. Ultrason. Ferroelectr. Freq. Contr. 2007;54(12) 2446-2455.

[55] Auld BA. Acoustic fields and waves in solids. Krieger; 1990.

[56] McHale G, Newton MI, Matin F. Layer guided shear horizontally polarized acoustic plate modes. Appl. Phys. Lett. 2002;91 5735.

[57] Wang Z, Cheeke JDN, Jen CK. Sensitivity analysis for Love mode acoustic gravimetric sensors. Appl. Phys. Lett. 1994;64(22) 2940-2942.

[58] Liu J and He S. Theoretical analysis on Love waves in layered structure with a piezoelectric substrate and multiple elastic layers. J. Appl. Phys. 2010;107 073511.

[59] Sankaranarayanan SKRS, Bhethanabotla VR, Joseph B. Modeling of Surface Acoustic Wave Sensor Response. In: Ram MK, Bhethanabotla VR. (ed.) Sensors for Chemical and Biological Applications. CRC Press; 2010. p97-134.

[60] Laude V, Reinhardt A, Ballandras S, Khelif A. Fast FEM/BEM computation of SAW harmonic admittance and slowness curves. In: proceedings of the IEEE Ultrason.Symp., 2004.

[61] Plessky VP and Thorvaldsson T. Rayleigh waves and leaky SAW's in periodic systems of electrodes: Periodic Green functions analysis. Electronics Letters 1992;28 1317-1319.

[62] Atashbar MZ, Bazuin BJ, Simpeh M, Krishnamurthy S. 3D FE simulation of H_2 SAW gas sensor. Sens. Actuators, B 2005;111-112 213-218.

[63] Xu G. Finite element analysis of second order effects on the frequency response of a SAW device. In: proceedings of the IEEE Ultrason.Symp., 2000.

[64] Ippolito SJ, Kalantar-Zadeh K, Powell DA, Wlodarski W. A 3-dimensional finite element approach for simulating acoustic wave propagation in layered SAW devices. In: proceedings of the IEEE Ultrason.Symp., 2003.

[65] Rocha-Gaso M-I, Fernandez-Díaz R, March-Iborra C, Arnau-Vives A. Mass sensitivity evaluation of a Love wave sensor using the 3D Finite Element Method. In: proceedings of the IEEE Int.Freq.Control Symp., 2010.

[66] Jakoby B and Vellekoop MJ. Properties of Love waves: applications in sensors. Smart Mater. Struct. 1997;6 668-679.

[67] Ferrari V and Lucklum R. Overview of Acoustic-Wave Microsensors. In: Arnau A. (ed.) Piezoelectric transducers and applications. Springer; 2008. p39-59.

[68] Lee HJ, Namkoong K, Cho EC, Ko C, Park JC, Lee SS. Surface acoustic wave immunosensor for real-time detection of hepatitis B surface antibodies in whole blood samples. Biosens. Bioelectron. June2009;24(10) 3120-3125.

[69] Kovacs G and Venema A. Theoretical comparison of sensitivities of acoustic shear wave modes for (bio) chemical sensing in liquids. Appl. Phys. Lett. 1992;61(6) 639-641.

[70] MacDougall D, Amore FJ, Cox GV, Crosby DG, Estes FL, et.al. Guidelines for data acquisition and data quality evaluation in environmental chemistry. Anal. Chem. 1980;52(14) 2242-2249.

[71] Du J, Harding DR, Collings AF, Dencher PR. An experimental study of Love-wave acoustic sensors operating in liquids. Sens. Actuators, A 1997;60 54-61.

[72] Gronewold TM. Surface acoustic wave sensors in the bioanalytical field: recent trends and challenges. Anal. Chim. Acta Nov.2007;603(2) 119-128.

[73] Jakoby B and Vellekoop MJ. Viscosity sensing using a Love-wave device. Sens. Actuators, A 1998;68 275-281.

[74] Francis LA, Friedt J-M, Bartic C, Campitelli A. A SU-8 liquid cell for surface acoustic wave biosensors. In: proceedings of the SPIE - The International Society for Optical Engineering, 2004.

[75] Tarbague H, Lachaud L, Vellutini L, Pillot JP, Bennetaur B, Moynet D, Rebière D. PDMS microfluidic chips combined to saw biosensors for ultra-fast biodetection of antibodies and E. coli bacteria. In: proceedings of the Biosensors 2012, Cancun, Mexico. 2012.

[76] Fournel F, Baco E, Mamani-Matsuda M, Degueil M, Bennetau B, Moynet D, Mossalayi D, Vellutini L, Pillot J-P, Dejous C, Rebiere D. Love wave biosensor for real-time detection of okadaic acid as DSP phycotoxin. In: proceedings of the Eurosensors XXIV, Linz, Austria. 2010.

[77] Kovacs G, Lubking GW, Vellekoop MJ, Venema A. Love waves for (bio)chemical sensing in liquids. In: proceedings of the IEEE Ultrason.Symp., Tucson, USA. 1992.

[78] Gizeli E, Goddard NJ, Lowe CR, Stevenson AC. A Love plate biosensor utilising a polymer layer. Sens. Actuators, B 1992;6 131-137.

[79] Freudenberg J, Schelle S, Beck K, von Schickfus M., Hunklinger S. A contactless surface acoustic wave biosensor. Biosens. Bioelectron. 1999;14 423-425.

[80] Howe E and Harding G. A comparison of protocols for the optimisation of detection of bacteria using a surface acoustic wave (SAW) biosensor. Biosens. Bioelectron. 2000;15(11-12) 641-649.

[81] Schlensog MD, Thomas MA, Gronewold TM, Tewes M, Famulok M, Quandt E. A Love-wave biosensor using nucleic acids as ligands. Sens. Actuators, B 2004;101 308-315.

[82] Moll N, Pascal E, Dinh DH, Lachaud J-L, Vellutini L, Pillot J-P, Rebière D, Moynet D, Pistré J, Mossalayi D, Mas Y, Bennetau B, Déjous C. Multipurpose Love acoustic wave immunosensor for bacteria, virus or proteins detection. ITBM-RBM 2008;29 155-161.

[83] Andrä J, Böhling A, Gronewold TMA, Schlecht U, Perpeet M, Gutsmann T. Surface acoustic wave biosensor as a tool to study the interactions of antimicrobial peptides with phospholipid and lipopolysaccharide model membranes. Langmuir 2008;24(16) 9148-9153.

[84] Bisoffi M, Hjelle B, Brown DC, Branch DW, Edwards TL, Brozik SM, Bondu-Hawkins VS, Larson RS. Detection of viral bioagents using a shear horizontal surface acoustic wave biosensor. Biosens. Bioelectron. Apr.2008;23(9) 1397-1403.

[85] El Fissi L, Friedt J-M, Luzet V, Chérioux F, Martin G, Ballandras S. A Love-wave sensor for direct detection of biofunctionalized nanoparticles. IEEE 2009; 861-865.

[86] Gammoudi I, Tarbague H, Lachaud JL, Destor S, Othmane A, Moyenet D, Kalfat R, Rebiere D, Dejous C. Love Wave Bacterial Biosensors and Microfluidic Network for Detection of Heavy Metal Toxicity. Sensor Letters 2011;9(2) 816-819.

[87] Song T, Song SY, Yoon HC, Lee K. Development of a wireless Love wave biosensor platform for multi-functional detection. Japanese J. of Appl. Phys. 2011;50 1-6.

[88] Kardous F, El Fissi L, Friedt J-M, Bastien F, Boireau W, Yahiaoui R, Manceau JF, Ballandras S. Integrated active mixing and biosensing using low frequency vibration mixer and Love-wave sensor for real time detection of antibody binding event. J. Appl. Phys. 2011;109 1-8.

[89] Tsortos A, Papadakis G, Mitsakakis K, Melzak KA, Gizeli E. Quantitative determination of size and shape of surface-bound DNA using an acoustic wave sensor. Biophys. J. 2008;94 2706-2715.

[90] Papadakis G, Tsortos A, Gizeli E. Triple-helix DNA structural studies using a Love wave acoustic biosensor. Biosens. Bioelectron. 2009;25 702-707.

[91] Gizeli E, Lowe CL, Liley M, Vogel H. Detection of supported lipid layers with the acoustic Love waveguidedevice: application to biosensors. Sens. Actuators, B 1996;34 295-300.

[92] Marth M, Maier D, Stahl U, Rapp M, Wessa T, Honerkamp J. Optimization of surface acoustic wave sensor arrays and application to high performance liquid chromatography. Sens. Actuators, B 1999;61 191-198.